

# PERFORMANCE–ENERGY TRADEOFFS IN CUTSET WIRELESS SENSOR NETWORKS

Matthew A. Prelee and David L. Neuhoff

EECS Department, University of Michigan, Ann Arbor, MI 48109

## ABSTRACT

This work explores performance vs. communication energy tradeoffs in wireless sensor networks that use the recently proposed *cutset* deployment strategy in which sensors are placed densely along a grid of intersecting lines. For a given number of sensors, intersensor spacing is less for a cutset network than for a conventional lattice deployment, so that cutset networks require less communication energy, albeit with some potential loss in network performance. Previous work analyzed the energy–performance tradeoffs for square-grid cutset networks in the context of specific decentralized algorithms for source localization based on received signal strength (RSS). The current work also considers the RSS based source localization problem. However, it takes a more fundamental approach to analyzing the tradeoff by considering a centralized task, minimum energy communication paths, Maximum Likelihood estimation algorithms and Cramér-Rao bounds. Moreover, it analyzes triangular and honeycomb cutset deployments, in addition to square-grid ones. The results indicate that cutset networks offer sizable decreases in energy with only modest losses of performance.

*Index Terms*— Wireless sensor networks, source localization.

## 1. INTRODUCTION

A common topic of research in the area of wireless sensor networks is that of finding ways to reduce energy consumption of battery-powered sensors, thereby increasing the overall lifetime of the network. For fixed hardware constraints, network energy consumption can be reduced by using efficient communication protocols [1–3], distributed algorithms [4, 5], and sensor-placement strategies [6, 7]. Recently, variants on all three of the above strategies were proposed to reduce the energy required in solving a single source, received-signal-strength (RSS)-based localization problem [8]. The authors proposed using a *Manhattan grid* sensor layout where sensors are placed along evenly-spaced rows and columns, as shown in Figure 1(e), and showed that in the context of specific decentralized estimation and communication strategies, this permitted a tradeoff in which communication energy could be substantially reduced with only modest decreases in performance. Previously, the Manhattan grid topology was also used in image processing applications, such as 2D bilevel lossy and lossless image coding [9–11] and grayscale image reconstruction [12, 13]. A sampling theorem for Manhattan grids has also been derived [14]. The problem of RSS-based source localization is similar to these image processing problems in that one is given noisy samples of an RSS “image” on the Manhattan grid, and the goal is to reconstruct properties of that image (in this case, the location of the source).

The current work again considers the RSS-based source localization problem. However, it takes a more fundamental approach to analyzing the tradeoff by considering a centralized task, minimum energy communication paths, Maximum Likelihood (ML) estima-

tion algorithms and Cramér-Rao bounds. Moreover, it analyzes triangular and honeycomb cutset deployments, in addition to square-grid ones. The results again indicate that cutset networks offer sizable decreases in energy with only modest losses of performance.

We begin by analyzing communication energy advantages of cutset networks in Section 2 for a many-to-one communication task. In Section 3, we use the RSS-based source-localization problem to demonstrate tradeoffs between estimation error and energy for various network topologies under two different noise models. Average Cramér Rao bounds and results of an approximate ML algorithm are used to measure error performance; these experimental results are shown in Section 4. We conclude our findings in Section 5.

## 2. CUTSET NETWORKS

When analyzing sensor networks, it is common to assume that sensors are randomly distributed, as in Fig. 1(a). However, in some applications, the network designers are free to choose where sensors are placed, perhaps using one of the lattice layouts in Fig. 1(b,c,d). We show that these are not as efficient at transmitting data as the cutset networks shown in Figure 1(e,f,g), which are formed by first placing sensors at the vertices of square, triangular, and hexagonal tessellations, respectively, and then evenly placing  $k - 1$  sensors between each vertex. Figures 1(e,f,g) show cutset networks for  $k = 5$ .

We wish to compare networks with a common sensor density  $\rho$ . For fixed  $\rho$ , a cutset network of parameter  $k$  will have intersensor spacing  $\lambda$  given by Table 1, and the tessellating polygon will have side length  $k\lambda$ . Thus, for fixed  $\rho$ , as  $k$  increases, intersensor spacing  $\lambda$  decreases as  $\mathcal{O}(k^{-1/2})$ , but the tessellating cell area increases as  $\mathcal{O}(k)$ . When these cell areas are large, their center points become increasingly distant from the closest sensor, which can lead to decreasing performance in a typical signal processing task.

For tractability, we restrict networks to a circular region  $B_R = \{t : \|t\| \leq R\}$  of radius  $R$ . To generate a network with approximately 250 sensors, we set the target density to be  $\rho = 250/\pi R^2$ , place a first sensor at the origin, generate an infinite network with the desired geometry using the intersensor spacing  $\lambda$  in Table 1, and finally, truncate the network to  $B_R$ . As a result, the final number of sensors  $n$  may differ slightly from 250. Let  $\mathcal{X} = \{x_i \in B_R, i = 0, \dots, n - 1\}$  denote the set of sensor locations, with  $x_0$  denoting the sensor at the origin. For random deployments, we merely place 250 sensors randomly within  $B_R$ .

Our analysis assumes the following far-field communication model: Let  $\alpha$  be some communication path-loss exponent between 2 and 4. If two sensors are separated by distance  $d$  communicate at received power  $P_0$ , we model the required transmission energy as

$$w(d) = P_0 d^\alpha.$$

Now suppose all sensors wish to transmit one packet of data to the sensor at  $x_0$  in order to run a centralized algorithm or make a centralized decision. Each sensor  $x \in \mathcal{X}$  chooses a path, i.e., a sequence

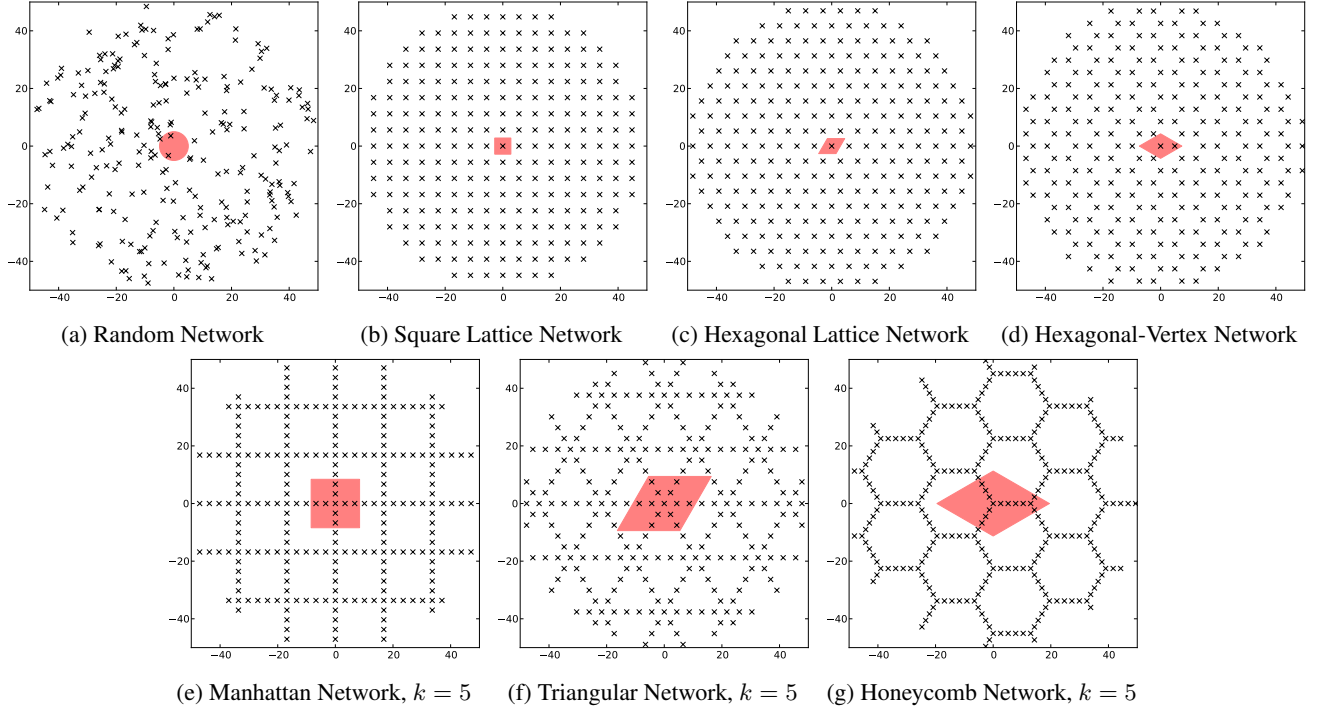


**Fig. 1:** Wireless networks with  $n \approx 250$  sensors placed in a circular region of radius  $R = 50\text{m}$ . The shaded region depicts possible locations of a randomly placed source in localization experiments. (a,b,c,d) show traditional network layouts; (e,f,g) show proposed *cutset networks*.

Network	$\rho$ : Density	$\lambda$ : Sensor Spacing	$c(r, \phi)$ : Min path cost	$\mathcal{E}_{int}$ : Energy estimate
Manhattan	$\frac{2k-1}{k^2\lambda^2}$	$\frac{1}{\sqrt{\rho}} \frac{\sqrt{2k-1}}{k}$	$\lambda^{\alpha-1} r ( \cos \phi  +  \sin \phi )$	$\frac{8}{3} \left( \frac{\sqrt{2k-1}}{k} \right)^{\alpha-1} \left( \frac{1}{\sqrt{\rho}} \right)^\alpha (R\sqrt{\rho})^3$
Triangular	$\frac{2}{\sqrt{3}} \frac{3k-2}{k^2\lambda^2}$	$\frac{1}{\sqrt{\rho}} \sqrt{\frac{2}{\sqrt{3}}} \frac{\sqrt{3k-2}}{k}$	$\lambda^{\alpha-1} r \left( \cos \phi + \frac{ \sin \phi }{\sqrt{3}} \right),  \phi  \leq \frac{\pi}{6}$	$\frac{4\sqrt{3}}{3} \left( \sqrt{\frac{2}{\sqrt{3}}} \frac{\sqrt{3k-2}}{k} \right)^{\alpha-1} \left( \frac{1}{\sqrt{\rho}} \right)^\alpha (R\sqrt{\rho})^3$
Honeycomb	$\frac{2}{3\sqrt{3}} \frac{3k-1}{k^2\lambda^2}$	$\frac{1}{\sqrt{\rho}} \sqrt{\frac{2}{3\sqrt{3}}} \frac{\sqrt{3k-1}}{k}$	$\frac{4}{3} \lambda^{\alpha-1} r \cos \phi,  \phi  \leq \frac{\pi}{6}$	$\frac{8}{3} \left( \sqrt{\frac{2}{3\sqrt{3}}} \frac{\sqrt{3k-1}}{k} \right)^{\alpha-1} \left( \frac{1}{\sqrt{\rho}} \right)^\alpha (R\sqrt{\rho})^3$

**Table 1:** Network quantities for  $P_0 = 1$ . Note that  $c(r, \phi)$  is  $\frac{\pi}{3}$  periodic for Triangle and Honeycomb networks.

of sensor locations  $x_{i_0} = x, x_{i_1}, x_{i_2}, \dots, x_{i_m}$  in  $\mathcal{X}$ , to relay its data to  $x_0$ , engendering a path cost equal to  $P_0 \sum_{j=1}^m \|x_{i_j} - x_{i_{j-1}}\|^\alpha$ , and a total energy that is the sum of such over all  $x \in \mathcal{X}$ . It is possible to compute the minimum possible total communication energy consumed by the network. First, form the complete weighted graph  $G = (\mathcal{X}, \mathcal{X} \times \mathcal{X}, W)$ , where  $W$  is the weighting matrix containing costs of direct communication between sensor nodes  $i$  and  $j$ , i.e.  $[W]_{ij} = w(\|x_i - x_j\|)$ . Dijkstra's algorithm [15] is then used to compute a set of minimum cost paths from the central node to all other nodes requiring  $\mathcal{O}(n^2)$  operations; the total minimum cost  $\mathcal{E}_{true}$  is then the total sum of weights along each of these paths. Note that because our assumed  $\alpha$  is greater than one, all hops in any optimal path in a cutset network will connect neighboring sensors.

This cost can be estimated using fewer computations. Suppose we are given a function  $c(r, \phi)$  that estimates the cost of transmitting a packet from a sensor at radius  $r$  and angle  $\phi$  to the central node  $x_0 = 0$ . The total minimum energy is approximately

$$\mathcal{E}_{true} \approx \mathcal{E}_{sum} \triangleq \sum_{i=1}^n c(\|x_i\|, \angle x_i).$$

This sum requires  $\mathcal{O}(n)$  operations. Expressions for  $c(r, \phi)$  for three different cutset networks are given in Table 1. These expressions are

derived under the assertion that all minimum cost paths follow the cell boundaries of the tessellation that generated the cutset network. If  $n$  is large (specifically, the density  $n/\pi R^2$  is large), then we may be able to model its local sensor density with some  $\rho(r, \phi)$ . The total minimum energy is approximately

$$\mathcal{E}_{true} \approx \mathcal{E}_{int} \triangleq \int_0^R \int_0^{2\pi} \rho(r, \phi) c(r, \phi) r dr d\phi.$$

For large networks based on tessellations, we approximate  $\rho(r, \phi)$  as a constant  $\rho$  and derive closed-form expressions for  $\mathcal{E}_{int}$ ; these are given in Table 1. When  $k$  is large and  $k, R, \rho$  and  $\alpha$  are fixed, honeycomb networks require the least energy. Specifically, Manhattan networks and triangular networks require  $3^{(\alpha-1)/4}$  and  $\frac{1}{2}3^{\alpha/2}$  times more energy than honeycomb networks, respectively.

Fig. 2 compares the output of Dijkstra's algorithm to the sum and integral approximations for  $\rho = 250/\pi R^2$  and  $R = 50\text{m}$ . These approximations performed reasonably well. As expected, the honeycomb networks outperformed the other networks for fixed  $k$ . A misleading part of Fig. 2 is that the honeycomb network consumed less energy than predicted and required more energy for  $k = 5$  than 4. This occurred because the  $k = 4$  network contained only 235 sensors, whereas the  $k = 5$  network contained 259. Actually, because  $\lambda$  decreases, the energy-per-sensor decreased from  $k = 4$  to  $k = 5$ .

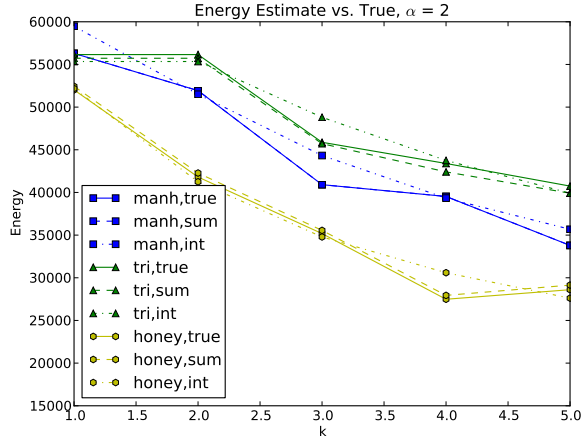


**Fig. 2:** Energy estimates for  $n \approx 250$  and  $k = \{1, 2, 3, 4, 5\}$ . All sum approximation estimates (2) had no more than 3% error, and all integral approximation estimates (2) had no more than 12% error.

We suspect two phenomenon contribute to the energy efficiency of honeycomb networks; both are derived from the assertion that cheapest paths in cutset networks lie along tessellation edges. First, the recently proven [16] “honeycomb conjecture” states that “any partition of the plane into regions of equal area has perimeter at least that of the regular hexagonal honeycomb tiling” [16]. Combining this with our assertion suggests that the sensor spacing  $\lambda$  may be smallest for honeycomb networks at fixed  $k$  and density  $\rho$ . Secondly, the cheapest communication path typically deviates less from an ideal straight-line path for Honeycomb networks than for the other networks. These hypotheses warrant further investigation.

### 3. NOISE MODELS FOR ENERGY-BASED SINGLE SOURCE LOCALIZATION

Let us now investigate the performance of cutset networks in the source localization problem. Suppose a source at location  $\theta \in B_R$  is emitting electromagnetic or acoustic waves. Our goal is to estimate  $\theta$  using noisy measurements of the received signal strength. Let  $\bar{\mathbf{y}}(\theta) \in \mathbb{R}_+^n$  denote a vector of RSS at the sensor nodes under no noise. If the sensors are sufficiently far apart (no closer than some  $\epsilon > 0$ ), we can assume the following far-field sensing model, where the  $i$ th element of  $\bar{\mathbf{y}}(\theta)$  is modeled according to

$$\bar{y}_i(\theta) = \frac{A}{\|x_i - \theta\|^\beta},$$

where  $A$  is the reference power of the signal at one meter and  $\beta$  is some sensing path-loss exponent, typically between 2 and 4 [17].

We consider two noise models: the Additive White Gaussian Noise (AWGN) model and the log-normal (LN) model. Excellent descriptions of both models are given in [17, 18]. Under the AWGN model, the observed RSS at node  $i$  is

$$y_i = \bar{y}_i(\theta) + u_i,$$

where each  $u_i$  is zero-mean i.i.d. Gaussian noise with variance  $\sigma^2$ . Thus, our observations  $\mathbf{y} = [y_i]_{i=1}^n$  are distributed as  $\mathcal{N}(\bar{\mathbf{y}}(\theta), \sigma^2 I)$ . In our experiments, we thresholded any negative  $y_i$  value to zero in order to avoid negative RSS readings.

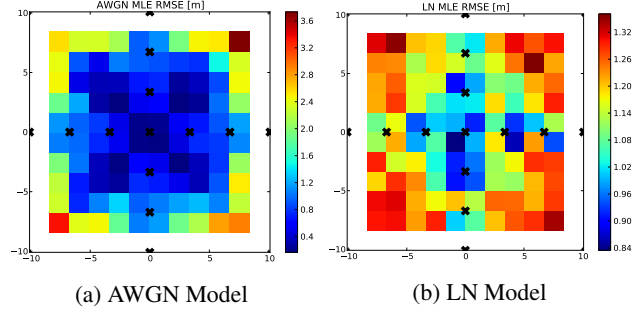


**Fig. 3:** MLE error distribution for Manhattan grid with  $n \approx 250$  sensors and  $k = 5$ , search window of circle of radius 30, coarse search resolution 0.15m, fine search resolution 0.01m, 20000 trials.

The log-normal model is slightly more realistic than the AWGN model, as it has been observed in practice [19–22] and derived analytically [23]. Under the LN model, observations are Gaussian in the log domain, i.e. the RSS in dB at the  $i$ th sensor node is

$$y_{i,db} = 10 \log_{10} \bar{y}_i(\theta) + v_i,$$

where each  $v_i$  is zero-mean i.i.d. Gaussian noise with known standard deviation  $\sigma_{db}$ . Our vector of observations  $\mathbf{y}_{db} = [y_{i,db}]_{i=1}^n$  is normally distributed as  $\mathcal{N}(10 \log_{10} \bar{\mathbf{y}}(\theta), \sigma_{db}^2 I)$ , where the  $\log_{10}$  is an abuse of notation denoting an element-wise logarithm. The standard deviation  $\sigma_{db}$  is typically observed to be between 4 and 12 [20].

#### 3.1. Cramér–Rao Bounds

We briefly derive the Cramér–Rao bounds (CRB’s) for these models. The reader may refer to [17, 18] for more thorough derivations.

Our goal is to estimate  $\theta = [\theta_1, \theta_2]^T$  from RSS observations  $y_i$ . If  $\mathbf{z}$  is a random vector distributed as  $\mathcal{N}(\boldsymbol{\mu}(\theta), \sigma^2 I)$ , then the  $jk$ -th element of the Fisher information matrix  $F$  is

$$[F]_{jk} = \frac{1}{\sigma^2} \frac{\partial \boldsymbol{\mu}^T}{\partial \theta_j} \frac{\partial \boldsymbol{\mu}}{\partial \theta_k}.$$

The variance of any unbiased estimator of the  $j$ th unknown coordinate  $\hat{\theta}_j$  given some observations  $\mathbf{z}$  is lower bounded according to  $\text{Var}(\hat{\theta}_j) \geq [F^{-1}]_{jj}$ ; this is known as the *Cramér–Rao Bound*. Under the AWGN model,  $\mathbf{z} = \bar{\mathbf{y}}$  and

$$\frac{\partial \bar{y}_i}{\partial \theta_j} = \beta A \frac{(x_{ij} - \theta_j)}{\|x_i - \theta\|^{\beta+2}}.$$

Similarly, under the LN model,  $\mathbf{z} = 10 \log_{10} \bar{\mathbf{y}}(\theta)$ , and

$$\frac{\partial (10 \log_{10} \bar{y}_i)}{\partial \theta_j} = \frac{10\beta}{\ln 10} \frac{(x_{ij} - \theta_j)}{\|x_i - \theta\|^2}.$$

These derivatives are easily computable, and the CRB can be calculated via an inversion of the  $2 \times 2$  Fisher information matrix  $F$ .

#### 3.2. Maximum Likelihood Estimation

Given some or all sensor observations  $y_i$ , under both noise models, the maximum likelihood (ML) solution can be found by minimizing the negative-log likelihood function. Under the AWGN model, the ML solution is given by solving the nonlinear least-squares problem

$$\hat{\theta}_{ML} = \underset{\theta}{\text{argmin}} \sum_{i=1}^n [y_i - \bar{y}_i(\theta)]^2.$$

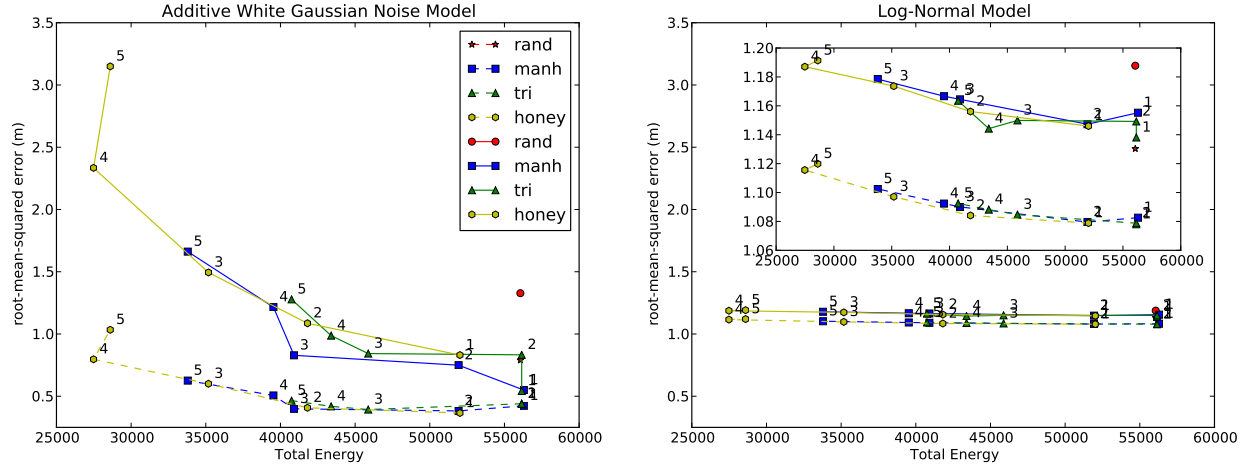


**Fig. 4:** Experimental results for MLE and CRB experiments for both noise models. Solid lines indicate MLE, and dashed lines indicate CRB. The log-normal plot includes a zoomed-in plot for closer comparison. The numbers along each data point indicate the  $k$  value of the network.

Similarly, under the LN model, the ML solution is given by

$$\hat{\theta}_{ML} = \underset{\theta}{\operatorname{argmin}} \sum_{i=1}^n [y_{i,db} - 10 \log_{10} \bar{y}_i(\theta)]^2.$$

In centralized applications, all sensor data is transmitted to a central node or fusion center. Any methods provided in [18] can be used to solve this ML problem. We implemented their multiresolution search method, where  $\hat{\theta}_{ML}$  is calculated by substituting a large number of candidate  $\theta$  values on a grid, first at a coarse search resolution, and then at a fine resolution centered at the coarse estimate.

#### 4. EXPERIMENTAL RESULTS

To compare the performance of various networks, we followed the following procedure. For a circular region  $B_R$  with radius  $R = 50$ , we generated networks of network density  $\rho = 250/\pi R^2$  according to the process in Section 2. For a random network (Fig. 1(a)), the sensor positions were randomized for each trial. For deterministic networks, we generated Manhattan, triangular and honeycomb networks with  $k = \{1, 2, 3, 4, 5\}$ . Note that  $k = 1$  corresponds to the lattices shown in Fig. 1(b,c,d), and a triangular network with  $k = 1$  is equivalent to a triangular network with  $k = 2$  at the same density. Cutset networks with  $k = 5$  are shown in Fig. 1(e,f,g). Energy usage was measured by calculating  $\mathcal{E}_{true}$  using Dijkstra's Algorithm, as described in Section 2. For each network type, 10,000 trials were performed for both the AWGN and LN noise models using reference powers  $A = 100$ , sensing path-loss  $\alpha = 2$ , communication path-loss  $\beta = 2$ , communication received-power  $P_0 = 1$ , AWGN noise variance  $\sigma^2 = 1$ , and log-normal noise standard deviation  $\sigma_{db} = 4$ .

In each trial, a random theta was placed uniformly near the center of the network within the red shaded regions in Fig. 1. The CRB was calculated for the current  $\theta$  value, a new realization of noisy data was generated, and the multiresolution MLE algorithm was performed to obtain an estimate  $\hat{\theta}_{ML}$  using a coarse grid search of 1m over the entire network, followed by a fine grid search of 0.01m centered at the coarse estimate. Upon completion of all trials, the average CRB along each coordinate  $\theta_1$  and  $\theta_2$  was calculated, and then the root-sum of these two average CRB's was computed, obtaining a lower bound on Root Mean Squared Error (RMSE) under a uniform

prior for  $\theta$ . Additionally, the RMSE of the ML estimates were calculated. The results for both noise models are plotted in Figure 4. Figure 3 shows the results of an additional experiment designed to show the distribution of MLE errors for a  $k = 5$  Manhattan grid.

Figure 4 shows how cutset networks offer significant increases in energy efficiency over random networks and lattice networks without surrendering much accuracy. This is shown in both the results of the MLE experiments and the average CRB calculations. The honeycomb networks with  $k = 4$  had the greatest gains in energy efficiency, offering a factor of 2 improvement over random networks and lattices. These energy gains are even more significant for larger values of the communication path-loss exponent  $\alpha$ . We note that an explanation was given in Section 2 for why energy increased from  $k = 4$  to 5 for honeycomb networks. Finally, as expected, Figure 3 shows how MLE performed much better near the intersection of Manhattan grid lines, and much worse near the center of squares where the distance to the nearest sensor was maximized.

#### 5. CONCLUSIONS AND ACKNOWLEDGMENTS

Previously, it was found that Manhattan grid sensor deployments allow for a significant reduction in communication energy over random or lattice deployments with only a modest loss in error performance for the problem of decentralized RSS localization [8]. This new work provides analytical and experimental evidence for an identical performance-energy tradeoff, but in the context of a centralized RSS localization problem. Furthermore, in addition to Manhattan grid networks, this tradeoff is also observed in triangular and honeycomb networks. In particular, our results suggest that there may be a fundamental advantage of honeycomb networks over other networks in terms of energy efficiency, which should be further investigated in future research. More efficient, decentralized algorithms for solving the source localization problem in cutset networks, such as the algorithm in [8], should also be investigated. Finally, future work should consider communication issues in cutset networks, such as scheduling, routing, and bounds on network throughput.

The authors would like to thank Robert P. Dick of the University of Michigan EECS department for his helpful insights.

## 6. REFERENCES

- [1] W.R. Heinzelman, A. Chandrakasan, and H. Balakrishnan, "Energy-efficient communication protocol for wireless microsensor networks," in *Proc. IEEE Annu. Hawaii Int. Conf. Sys. Sci.*, Jan. 2000, pp. 1–10.
- [2] W. Ye, J. Heidemann, and D. Estrin, "An energy-efficient mac protocol for wireless sensor networks," in *IEEE INFOCOM*, June 2002, pp. 1567–1576.
- [3] T. Van Dam and K. Langendoen, "An adaptive energy-efficient mac protocol for wireless sensor networks," in *Proc. ACM Int. Conf. Embedded Networked Sensor Systems*, Nov. 2003, pp. 171–180.
- [4] M.G. Rabbat and R.D. Nowak, "Decentralized source localization and tracking," in *IEEE ICASSP*, Montreal, May 2004, pp. iii–921.
- [5] D. Blatt and A.O. Hero, "Energy-based sensor network source localization via projection onto convex sets," *IEEE Trans. Sig. Proc.*, vol. 54, no. 9, pp. 3614–3619, 2006.
- [6] A. Salhieh, J. Weinmann, M. Kochhal, and L. Schwiebert, "Power efficient topologies for wireless sensor networks," in *IEEE Int. Conf. Parallel Proc.*, Sept. 2001, pp. 156–163.
- [7] P. Cheng, C. Chuah, and X. Liu, "Energy-aware node placement in wireless sensor networks," in *IEEE GLOBECOM*, Nov. 2004, pp. 3210–3214.
- [8] M.A. Prelee and D.L. Neuhoff, "Energy efficient source localization on a manhattan grid wireless sensor network," in *Proc. IEEE ICASSP*, Vancouver, May 2013, pp. 4266–4270.
- [9] M.G. Reyes, X. Zhao, D.L. Neuhoff, and T.N. Pappas, "Lossy compression of bilevel images based on markov random fields," in *Proc. IEEE ICIP*, San Antonio, Sept. 2007, vol. 2, pp. II–373.
- [10] M.G. Reyes and D.L. Neuhoff, "Arithmetic encoding of markov random fields," in *Proc. IEEE Int. Symp. Inform. Thy.*, Seoul, June 2009, pp. 532–536.
- [11] M.G. Reyes and D.L. Neuhoff, "Lossless reduced cutset coding of markov random fields," in *Proc. Data Compression Conf.* Mar. 2010, pp. 386–395, Snowbird.
- [12] A. Farmer, A. Josan, M.A. Prelee, D.L. Neuhoff, and T.N. Pappas, "Cutset sampling and reconstruction of images," in *Proc. IEEE ICIP*, Brussels, Sept. 2011, pp. 1909–1912.
- [13] M.A. Prelee, D.L. Neuhoff, and T.N. Pappas, "Image reconstruction from a manhattan grid via piecewise plane fitting and gaussian markov random fields," in *Proc. IEEE ICIP*, Orlando, FL, Sept. 2012, pp. 2061–2064.
- [14] M.A. Prelee and D.L. Neuhoff, "A sampling theorem for manhattan grids," in *Proc. IEEE ICASSP*, Kyoto, Mar. 2012, pp. 3797–3800.
- [15] E.W. Dijkstra, "A note on two problems in connexion with graphs," *Numerische mathematik*, vol. 1, no. 1, pp. 269–271, 1959.
- [16] T.C. Hales, "The honeycomb conjecture," *Discrete & Computational Geometry*, vol. 25, no. 1, pp. 1–22, 2001.
- [17] N. Patwari, J.N. Ash, S. Kyperountas, A.O. Hero III, R.L. Moses, and N.S. Correal, "Locating the nodes: cooperative localization in wireless sensor networks," *IEEE Sig. Proc. Magazine*, vol. 22, no. 4, pp. 54–69, 2005.
- [18] X. Sheng and Y.H. Hu, "Maximum likelihood multiple-source localization using acoustic energy measurements with wireless sensor networks," *IEEE Trans. Sig. Proc.*, vol. 53, no. 1, pp. 44–53, 2005.
- [19] N. Patwari, R.J. O’Dea, and Yanwei Wang, "Relative location in wireless networks," in *Proc. IEEE VTC*, May 2001, vol. 2, pp. 1149–1153.
- [20] T. Rappaport, *Wireless Communications: Principles and Practice*, Prentice Hall PTR, Upper Saddle River, NJ, USA, 2nd edition, 2001.
- [21] H. Hashemi, "The indoor radio propagation channel," *Proc. IEEE*, vol. 81, no. 7, pp. 943–968, 1993.
- [22] N. Patwari, A.O. Hero, M. Perkins, N.S. Correal, and R.J. O’Dea, "Relative location estimation in wireless sensor networks," *IEEE Trans. Sig. Proc.*, vol. 51, no. 8, pp. 2137–2148, 2003.
- [23] A.J. Coulson, A.G. Williamson, and R.G. Vaughan, "A statistical basis for lognormal shadowing effects in multipath fading channels," *IEEE Trans. Comm.*, vol. 46, no. 4, pp. 494–502, 1998.